J Nanopart Res (2018) 20: 223
https://doi.org/10.1007/s11051-018-4317-0

RESEARCH PAPER

Catalytic graphitization of kraft lignin to graphene-based structures with four different transitional metals

Qiangu Yan · Jinghao Li · Xuefeng Zhang · El Barbary Hassan · Chuji Wang · Jilei Zhang · Zhiyong Cai

Received: 23 May 2018 / Accepted: 31 July 2018 / Published online: 25 August 2018

Abstract Catalytic graphitization of kraft lignin to nano-materials was investigated over four transitional metal catalysts (Ni, Cu, Fe, and Mo) through a thermal treatment process under an argon flow at 1000 °C. The catalytic thermal process was examined using thermal gravimetric analysis (TGA) and temperature-programmed decomposition (TPD) experiments. The crystal structure and morphology of the thermal-treated metal-lignin samples were characterized by X-ray diffraction (XRD), scanning electron microscopy (SEM), high-resolution transmission electron microscopy (HRTEM), and Raman spectroscopy. Catalytic graphitization of kraft lignin to nano-materials was investigated over four transitional metal catalysts (Ni, Cu, Fe, and Mo) through a catalytic thermal treatment process. It was observed that multi-layer graphene-encapsulated metal nanoparticles were the main products, beside along with some graphene sheets/flakes. The particle sizes and graphene shell layers were significantly affected by the promoted metals. BET surface areas of samples obtained from different metal precursors were in the range of 88–115 m^2/g within the order of Ni- > Fe- > Mo- > Cu-. Thermal gravimetric analysis (TGA) and temperature-programmed decomposition (TPD) experimental results showed that adding transitional metals could promote the decomposition and carbonization of kraft lignin. The catalytic activity increased with an order of Mo≅Cu < Ni≅Fe. XRD results show that face-centered cubic (fcc) Cu crystals is formed in the thermal-treated Cu-lignin sample, fcc nickel phase for the Ni-lignin sample, β-Mo_2C hexagonal phase for the Mo-lignin sample and α-Fe, γ-iron, and cementite(Fe_3C) for the Fe-lignin sample. Average particle sizes of these crystal phases calculated using the Scherrer formula are 52.4 nm, 56.2 nm, 21.0 nm, 23.3 nm, 11.3 nm, and 32.8 nm for Ni, Cu, β-Mo_2C, α-Fe, γ-iron, and Fe_3C, respectively. Raman results prove that the graphitization activity of these four metals is in the order of Cu < Mo < Ni < Fe. Metal properties such as catalytic activity, carbon solubility, and tendency of metal carbide formation were related to the graphene-based structure formation during catalytic graphitization of kraft lignin process.

Keywords Kraft lignin · Catalytic graphitization · Transitional metals · Multi-layer graphene- encapsulated metal nanoparticles · Graphene sheets/flakes

Qiangu Yan and Jinghao Li contributed equally to this work.

Q. Yan · X. Zhang · E. B. Hassan · J. Zhang (✉)
Department of Sustainable Bioproducts, Mississippi State University, Mississippi State, MS 39762-9820, USA
e-mail: jz27@msstate.edu

J. Li · Z. Cai (✉)
Forest Products Laboratory, USDA Forest Service, One Gifford Pinchot Drive, Madison, WI 53726-2398, USA
e-mail: zcai@fs.fed.us

C. Wang
Department of Physics and Astronomy, Mississippi State University, Mississippi State, MS 39762-9820, USA

Introduction

Lignin is a low value by-product from wood pulping industries. Worldwide, approximately 50–70 and 2 million metric tons/year of kraft lignin and lignosulfonates are produced on an annual basis (Aro and Fatehi 2017). Lignosulfonates have a wide variety of applications; lignosulfonates are used to disperse pesticides, dyes, and carbon black; and lignosulfonates are also used as plasticizers in making concrete and as feedstock to make fine chemicals; however, the majority of kraft lignin is being used as a low-grade fuel for the kraft pulping process operation (Doherty et al. 2011). Researchers have tried to find better uses of kraft lignin, lignosulfonates, and other industrial lignins in past decades. Carbon contributes approximately 60% mass of lignin; therefore, lignin has been used as carbon precursor to produce templated carbons (Ruiz-Rosas et al. 2014), carbon fibers (Otani et al. 1969), and activated carbon (Suhas et al. 2007). Graphene materials have been synthesized from thermal treatment of a mixture of lignosulfonate and iron nanoparticles (Mun et al. 2013), where amorphous carbon from lignin was catalytically converted to ordered graphite structures over iron particles. Catalytic graphitization of solid carbon has been studied for several decades (Ōya and Ōtani 1979). Two mechanisms have been proposed for the formation of graphite from solid carbon substrates over metal catalysts: (1) The first possible mechanism is dissolution-precipitation process (Derbyshire et al. 1975; Weisweiler et al. 1971): at certain temperature, the disorder carbons tend to diffuse and dissolve into metal and/or metal carbide, and a saturated carbon solubility is reached under an equilibrium situation. With decreasing temperature, the metal saturated with the disordered carbon will be supersaturated with carbon. Consequently, carbon precipitates in the form of graphite crystals since graphite is highly ordered carbon with the lowest Gibbs free energy; (2) The second mechanism is metal carbide formation and decomposition process (Ōya and Ōtani 1979; Derbyshire et al. 1975; Weisweiler et al. 1971): a metal may first react with amorphous carbon to form metal carbides which can decompose to metal and graphite. Based on catalytic graphitization mechanisms, it is reasonable to classify the reactivity of the transition metals with carbon into three groups: (i) metals have very low carbon solubility; (ii) metals can dissolve a significant carbon; (iii) metals may form strong chemical bonds with carbon to result in the metal carbides.

Transition metals are widely used as active components for carbonization/graphitization carbon sources to produce nano-structural carbons like graphene, carbon nanotubes, and carbon nanofibers (Wang et al. 2017; Ōya and Marsh 1982; Bacsa et al. 2015) The product structures may be affected by the active phase and reaction conditions. Researchers have reported previously on catalytic graphitization of solid carbon resources (Ōya and Ōtani 1979; Weisweiler et al. 1971; Yokokawa et al. 1966; Ishikawa and Yoshizawa 1963; Kakunuri et al. 2016; Maldonado-Hódar et al. 2000; Demir et al. 2015; Wang et al. 2016). Oya et al. studied the catalytic graphitization of 3,5-dimethylphenol-formaldehyde (3,5-DMPF) and phenol formaldehyde carbons over 22 metallic catalysts at 2600 °C for 1 h and 3000 °C for 10 min under argon atmosphere (Ōya and Ōtani 1979). Weisweiler et al. studied the graphitization of monolithic glass-like carbon as catalyzed by molten metals (Weisweiler et al. 1971). Yokokawa et al. investigated the catalytic graphitization of divinyl benzene polymer, furfuryl alcohol, or furfural between 1400 and 2300 °C with an addition of 5 wt% transitional metallic compounds of Cu, Ni, Co, Mn, Al, Ag, Zn, and Sn (Yokokawa et al. 1966). Ishikawa and Yoshizawa examined the effects of metallic compounds on graphitization of coke at temperatures between 2000 and 2500 °C (Ishikawa and Yoshizawa 1963). Kakunuri et al. reported the catalytic graphitization of resorcinol-formaldehyde (RF) xerogel at different temperatures ranging from 900 to 1800 °C (Kakunuri et al. 2016). Maldonado-Hódar et al. first prepared aerogels from polymerization of resorcinol with formaldehyde, then catalytic graphitization of these aerogels with Cr-, Fe-, Co-, and Ni metals at temperatures between 500 and 1800 °C (Maldonado-Hódar et al. 2000). Demir et al. produced graphitic porous carbon from lignin using a two-step process: lignin is first hydrothermal carbonized at 300 °C and 1500 psi to produce biochar, which is then graphitized using a metal nitrate (iron, cobalt, and manganese nitrates) catalysts at 900–1100 °C in an inert gas at 15 psi (Demir et al. 2015). Wang et al. examined the catalytic graphitization mechanism of coal-based carbon materials with light rare earth elements using X-ray diffraction, scanning electron microscopy, energy-dispersive X-ray spectroscopy, selected-area electron diffraction, and high-resolution transmission electron microscopy (Wang et al. 2016). Our previous work examined catalytic graphitization of kraft lignin using iron catalyst at 1000 °C in argon, hydrogen, CO_2,

methane, and natural gas atmospheres; experimental results showed that methane and natural gas accelerated the formation of multi-layer graphene materials, and an etching effect was observed for hydrogen and carbon dioxide, while multi-layer graphene-encapsulated iron nanoparticles were the main products in the case of argon (Yan et al. 2018).

In this work, a catalytic graphitization process of kraft lignin is proposed to produce graphene-based nano-materials over metal catalysts; four transitional metals, i.e., Fe, Ni, Mo, and Cu, are selected as the catalyst active components. The effect of transition metals Cu, Ni, Mo, and Fe on catalytic graphitization of kraft lignin to graphene materials is investigated. In the present study, the role of transition metals (Fe, Ni, Mo, and Cu) in the catalytic growth of graphene from kraft lignin is investigated through an experimental approach.

Experimental

Chemicals and materials

Copper nitrate tetrahydrate ($Cu(NO_3)_2{\cdot}4H_2O$), nickel nitrate hexahydrate ($Ni(NO_3)_2{\cdot}6H_2O$), ammonium molybdate tetrahydrate ($(NH_4)_6Mo_7O_{24}{\cdot}4H_2O$), iron(III) nitrate nonahydrate ($Fe(NO_3)_3{\cdot}9H_2O$), and tetrahydrofuran were purchased from Sigma-Aldrich, and kraft lignin was provided by Domtar Corporation.

The promotion of metal ions on the kraft lignin

The metal-kraft lignin precursors were prepared by the co-precipitation method as follows:

For the preparation of copper-promoted lignin: 100 g of kraft lignin was first added to 100 mL tetrahydrofuran in a 200-mL glass beaker and stirred for 2 h. Also, 42.7 g of copper nitrate tetrahydrate were added to 50 mL DI water in a 500-mL glass beaker and stirred for 30 mins. Following that, copper nitrate solution drop-like (~2 mL/min) was added to kraft lignin solution with continuous stirring for 2 h. The mixture was kept at room temperature for 24 h, and then transferred to an oven where it was dried at 110 °C for 24 h.

For the preparation of nickel-promoted lignin: 100 g of kraft lignin was first added to 100 mL tetrahydrofuran in a 2000-mL glass beaker and stirred for 2 h. Similarly, 56.2 g of nickel nitrate hexahydrate were added to 50 mL DI water in a 500-mL glass beaker and stirred for 30 mins. Following that, nickel nitrate solution drop-like was added to kraft lignin solution and stirred continuously for 2 h. The mixture was kept at room temperature for 24 h, and then transferred to an oven where it was dried at 110 °C for 24 h.

For the preparation of molybdenum promoted lignin: 100 g of kraft lignin was first added to 100 mL tetrahydrofuran in a 2000-mL glass beaker and stirred for 2 h. Similarly, 46.4 g of ammonium molybdate tetrahydrate were added to 100 mL DI water in a 500-mL glass beaker and stirred for 30 mins. Following that, ammonium molybdate solution drop-like was added to kraft lignin solution and stirred for 2 h. The mixture was kept at room temperature for 24 h, and then transferred to an oven where it was dried at 110 °C for 24 h.

For the preparation of iron promoted lignin: 300 g of kraft lignin was first added to 300 mL tetrahydrofuran in a 2000-mL glass beaker and stirred for 2 h. Also, 246 g of iron (III) nitrate nonahydrate is added to 100 mL DI water in a 500-mL glass beaker and stirred until it is dissolved completely. Following that, the iron nitrate solution drop-like was added to kraft lignin solution and stirred for 2 h. The mixture was kept at room temperature for 24 h, and then transferred to an oven where it was dried at 110 °C for 24 h.

Thermogravimetric analysis experiments

Thermogravimetric analysis of the samples was carried out in a thermogravimetric analysis (TGA) (Shimadzu TGA-50H) through isothermal analyses. The system was capable of quantitatively measuring the change in mass of a sample as a function of temperature up to 1500 °C. The change in mass was then related to the changes taking place in the sample during decomposition. For each sample prepared, argon (99.99% purity, 50 ml/min) flowed through the TGA at 50 mL/min as the temperature was ramped at 10 °C/min. Each sample was tested for at least three replicates.

Temperature-programmed decomposition

Temperature-programmed decomposition (TPD) experiments involved heating the sample in an argon purging gas (20 mL/min) at a programmed heating rate to induce thermal decomposition of metal-promoted samples. TPD experiments were carried out using an Autochem 2920. One gram (1 g) of the sample was used in each

run. Volatile species from the TPD process were measured with an on-line residue gas analyzer (RGA).

Graphene-based structures formation by thermal treatment of metal-lignin samples

Fifteen grams (15 g) of the metal-promoted kraft lignin samples were each packed in the middle of a 1-in. OD ceramic tubular reactor. The carrier gas argon (99.99% purity) was first introduced into the reactor at a flow rate of 80 mL/min for 30 min. The reactor was heated at a rate of 10 °C/min to 1000 °C and kept at 1000 °C for 1 h. The furnace was cooled down by 10 °C/min to room temperature under an argon flow. The product stream from the reactor passed through a gas-liquid separator, where the temperature was held at 0 °C. Liquid products were collected from the cold condenser. The gas phase product from the condenser was gathered by a gas tank and analyzed using an Agilent 6890 gas chromatograph (GC).

The selectivity of solid residue product was calculated by

$$X\% = \left(\frac{A}{B}\right) \times 100\% \tag{2.1}$$

where A was the weight of the solid residue after catalytic thermal treatment, and B was the weight of metal-promoted kraft lignin sample before thermal treatment.

The solid carbon selectivity was measured by TGA. Twenty milligrams of the solid residue (20 mg) gathered after catalytic thermal treatment was put on a ceramic sample pan for TPO analysis in a Shimadzu TGA-50H instrument. By heating the sample in high air flow of air (100 ml/min) from room temperature to 800 °C with 10 °C/min, the weight change was recorded as related to carbon burning. The selectivity of solid carbon product was calculated by

$$Y\% = X\%(C/D) \tag{2.2}$$

where C was the weight loss of the solid residue after TGA, and D was the weight of solid residue sample before TGA.

Characterization

X-ray powder diffraction (XRD) patterns of the samples were obtained using a Rigaku Ultima III X-ray Diffraction System operated at 40 kV and 44 mA using Cu-Kα radiation with a wavelength of 1.5406 Å, from 20° to 80° at a scan rate of 0 02°s^{-1}. The Jade powder diffraction analysis software from Materials Data, Inc. was used for both qualitative and quantitative analysis of polycrystalline powder materials. The morphology of the samples was investigated with a scanning electron microscope (SEM). All samples were pre-coated with 10 nm Pt before being introduced into the vacuum chamber. The system was operated with accelerating voltage of 10 kV. The sample particle sizes were examined with a JEOL JEM-100CX II transmission electron microscope (TEM) operated at accelerating voltage of 200 kV. All samples were sonicated in ethanol solution for 1 min before transferred to copper grids. Raman spectroscopy measurements were carried out using a Jobin-Yvon microspectrometer equipped with an excitation laser source emitting at 514 nm and an incident power around 1 mW on a thin surface. Twenty spectra were collected for each sample.

Results and discussion

TGA

Figure 1 shows the TG and DTG curves of the raw kraft lignin and the metal-kraft lignin samples. As shown in the TG/DTG curves, the thermal degradation of kraft lignin proceeded over a wide temperature range (150–1000 °C) (Fig. 1a). From 30 to 140 °C, almost 6.3% of the sample weight was lost, and mainly attributed to the evaporation of free water in the sample. The differential thermogravimetric (DTG) curve shows that between 150 and 534 °C there was a single maximum occurring at 436 °C, indicating of lignin decomposition. Weight loss in the range of 150–534 °C was about 46%, while weight loss between 534 and 1000 °C was 11.3%.

There are three significant mass loss steps shown in Fig. 1b (Cu-lignin sample). The first and highest mass loss of the copper-promoted lignin occurred in the temperature range from 71 to 385 °C with a peak temperature of 279 °C. There is about 33.5% mass loss in this step. The second loss of mass is found around 385 to 700 °C. The mass loss in this zone is 10%. After 700 °C until 1000 °C, the mass decreases gradually.

TG/DTG curves of Ni-lignin sample are plotted in Fig. 1c. As shown, the catalytic decomposition process

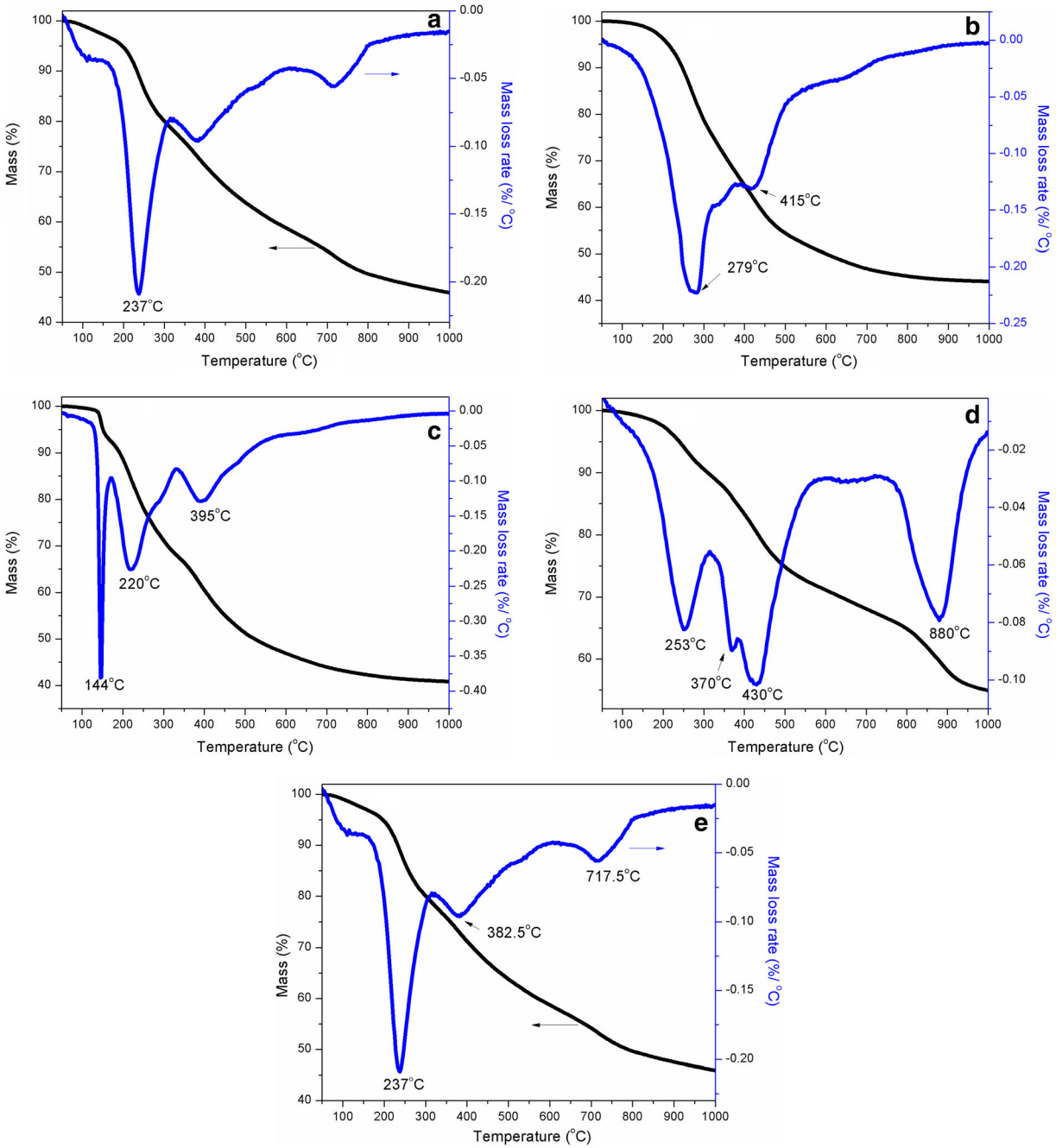

Fig. 1 TG and DTG curves of the raw kraft lignin and the metal-kraft lignin samples heated at a rate of 10 °C/min in argon atmosphere: **a** raw kraft lignin, **b** Cu-lignin, **c** Ni-lignin, **d** Mo-lignin, and **e** Fe-lignin

could be divided into four stages: (1) The first mass loss peak at 144 °C, which is attributed by water evaporation, (2) the second mass loss is centered at 220 °C, it is due to the decomposition of nickel nitrate and side chain structures de-polymerization, (3) the third mass loss stage is peaked at 320 °C, and (4) the fourth mass loss is between 600 and 1000 °C. Nickel has been known to be one of the efficient catalysts for the graphitization of amorphous carbons (Suhas et al. 2007; Yudasaka et al. 1997).

For lignin promoted by ammonium heptamolybdate, continuous gradual weight loss between 130 and 320 °C corresponds to the decomposition of ammonium heptamolybdate (Fig. 1d). At around 320–385 °C, the shoulder peak is attributed to the partial reduction of Mo^{3+} in ammonium heptamolybdate. The DTG curve of Fig. 1d shows that there is a mass loss peak at 430 °C. From 585 to 730 °C, around 4.38% of the mass loss corresponds to the reduction of Mo oxides to metallic Mo. The sharp peak at 880 °C is attributed to the formation of Mo_2C and lignin char is catalytic graphitization by molybdenum carbide.

The TG and DTG curves for the Fe-lignin sample are shown in Fig. 1e. There are four possible steps. The initial mass loss occurs between 50 and 160 °C with a tiny peak temperature of 112.5 °C. The second mass loss is observed around 160 to 317 °C. The maximum mass loss peak was centered at 237.5 °C. Figure 1e shows the mass loss of this stage was 13.71%. The maximum mass loss rate is 0.209%/°C at this point. The most mass loss occurs between 317 to 588 °C corresponding to the decomposition of kraft lignin char from the second stage. The peak temperature of the third stage is 382.5 °C with a mass loss rate of 0.096%/°C. The mass loss of this stage is 21.33%. The last mass loss stage is characterized with a further carbonization and graphitization process of the char residues in a wide temperature zone of 588 to 1000 °C. In this zone, mass loss is mainly attributed to the decomposition of phenols, quinine, ether, and C-H groups, which gives out CO and H_2 as the main products. The peak temperature of this stage is 710 °C with a mass loss rate of 0.0.056%/°C. The mass loss of the catalytic carbonization/graphitization stage is 13.32%.

TPD-MS

Figure 2a shows the evolution curves of some of the main gaseous products (CO_2, CO, CH_4, H_2S, and H_2) from decomposition of the kraft lignin. The release of CO_2 and CO at the lower temperature range below 500 °C was mainly a result of the cracking and reforming of carboxyl, carbonyl, and ether groups in the phenylpropane side chains. Both gases were initially released from kraft lignin at lower temperatures. The evolution of CO_2 started at approximately 350 °C, increased with increasing temperature, and reached a maximum at 400 °C for kraft lignin. Compared with CO_2, CO evolution is detected over a wider temperature range of 300–700 °C, with a formation peak at 500 °C. The formation of the carbon monoxide at high temperature range (450–700 °C) was probably caused by the breaking of diaryl ether groups and secondary pyrolysis of volatiles. The CO releasing peak at 700 °C was attributed to the break of diaryl ether linkages. The formation of methane below 550 °C was mainly caused by the fragmentation of the side chains. Demethylation of the methoxy groups could also contribute to methane formation in this temperature range, especially above about 400 °C. The second maximum of methane could be attributed to the breaking of aromatic rings.

Figure 2b shows the trends of the volatile gas species during temperature-programmed thermal treatment of the copper-promoted lignin sample. TPD curves were different from those of the raw lignin. A significant amount of gases like CO_2, CO, CH_4, and NO_2 were released in the temperature zone of 85–300 °C. This implied that copper ions promoted the de-polymerization of lignin. NO_2 peak was observed from 102 to 250 °C with a maximum at 160 °C. It meant the decomposition of copper nitrate occurred in this temperature range. In the prepared Cu-lignin precursor, Cu ions were combining with oxygen-containing functional groups like carboxyl, carbonyl, ester, or hydroxyl. Under thermal treatment process, copper nitrate decomposed and produced copper oxide, nitrogen dioxide, and oxygen ($2\ Cu(NO_3)_2 = 2\ CuO + 4\ NO_2 + O_2$). Copper ions and copper oxides trapped in the lignin matrix were reduced by CO, H_2, and the functional groups of the lignin, especially those of aliphatic side branches (for example -CH_2OH). Simultaneously, lignin was deconstructed, released volatile gas (i.e., CO_2, CO, H_2O, CH_4), and form solid char after the first stage ($CuO + lignin \rightarrow Char + Cu + CO_2 + CO + H_2O + CH_4$). After the first stage of catalytic de-polymerization (85–300 °C), metal copper particles were trapped in the solid char structure (Leng et al. 2017); with increased heating temperature, the reduced metallic copper nanoparticles served as the catalyst to carbonize char to carbon and gases ($Char \rightarrow Carbon + CO_2 + CO + H_2O + CH_4$).

Figure 2c shows the trends of vent gas species (CO_2, CO, CH_4, NO_2, and H_2) during temperature-programmed thermal treatment of the nickel-doped lignin sample. Like the Cu-lignin sample, TPD curves

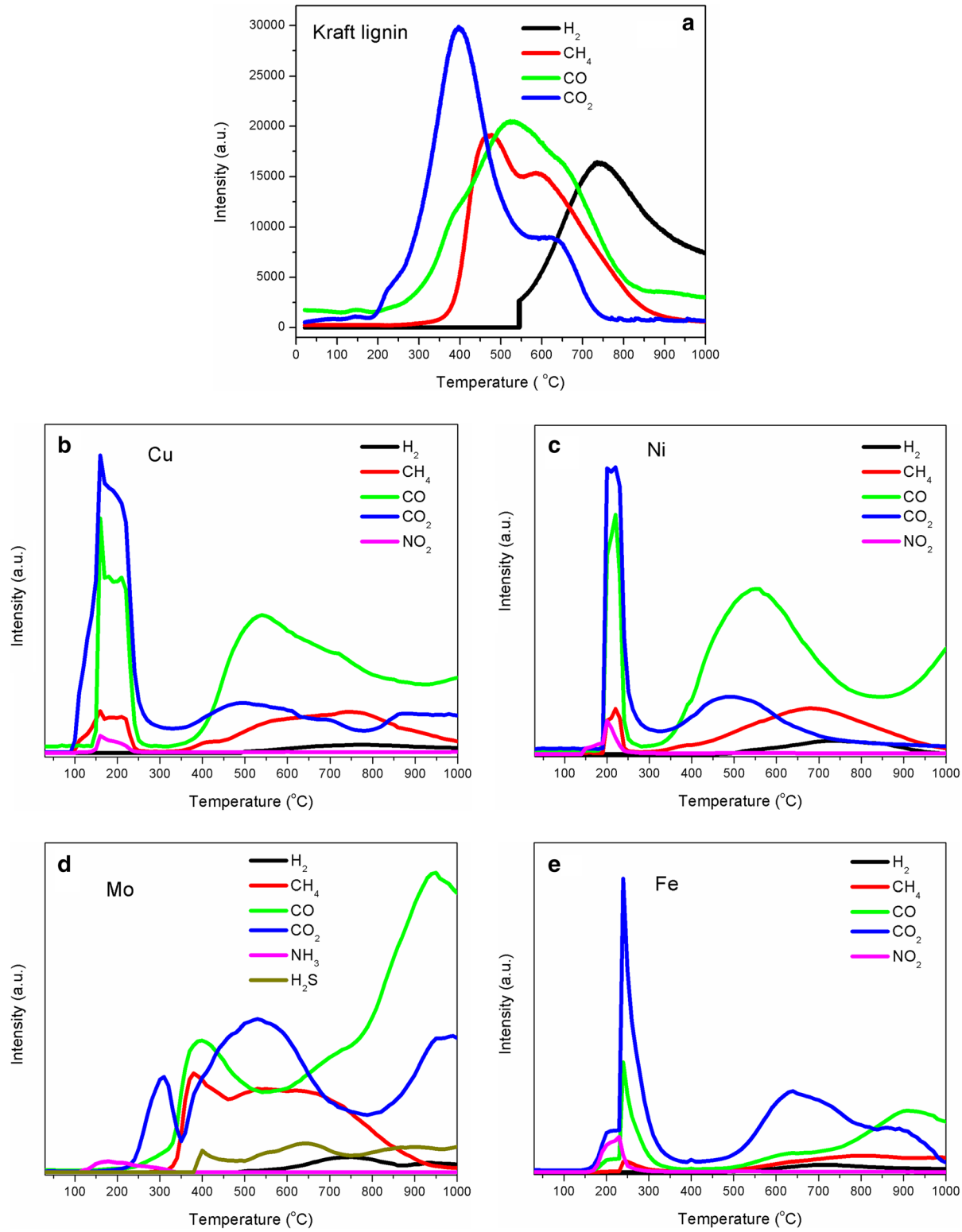

Fig. 2 Hydrogen, methane, carbon monoxide, carbon dioxide, ammonia, hydrogen sulfide, and nitrogen dioxide evolution for the temperature-programmed thermal treatment of kraft lignin and the different metal-promoted kraft lignin at a rate of 10 °C/min in argon atmosphere: **a** kraft lignin, **b** Cu, **c** Ni, **d** Mo, and **e** Fe

of Ni-lignin were also different compared to those of the kraft lignin. NO_2 was observed to appear from 138 °C with a maximum at 199.5 °C. Nickel(II) nitrate was thermally decomposed to produce nickel(II) oxide, nitric oxide, and oxygen ($2Ni(NO_3)_2 \rightarrow 2NiO + 4NO_2 + O_2$). Then CO_2, CO, and CH_4 were released in the temperature zone of 185–300 °C. This implied that the de-polymerization of lignin is associated with the promotion of nickel. The release of CO_2, CO, and CH_4 at the lower temperature range was mainly a result of the cracking and reforming of carboxyl, carbonyl, and ether groups in the phenylpropane side chains. The evolution of CO_2 began at approximately 185 °C, increased with increasing of temperature, and reached a maximum at 215 °C. Compared with CO_2, CO evolution was detected over a similar temperature range of 185–280 °C, with a maximum at about 218 °C. The formation of carbon monoxide at this temperature range was probably caused by the breaking of diaryl ether groups in kraft lignin. There was a small methane evolution peak between the temperature of 185 and 255 °C, and it was mainly caused by the fragmentation of the side chains. In the second stage, the formed char was catalytic carbonized to carbon from 300 to 1000 °C. The strong CO peak of 555 °C was assigned to ether decomposition. This implied that nickel ions promoted the hydrolysis of the ether. The weak intensity CO_2 peak at 490 °C was assigned to the carbothermal reduction of nickel oxide. Hydrogen evolution was observed when the temperature was above 490 °C; it was assigned to cracking of $–CH_x (x = 1–3)$ groups promoted by nickel metal. In the present work, nickel oxide dissolved in the lignin matrix was first reduced by H_2, CO, and surface functional groups of the lignin, then the reduced metallic nickel reacted with amorphous carbon to form carbon-encapsulated nickel nanoparticles (NiO + active functional groups → Ni + CO_2 + CO + H_2O).

Figure 2d shows the mass spectroscopy of the vent gas during the thermal decomposition of Mo-lignin sample. Hydrogen, methane, ammonia, carbon monoxide, hydrogen sulfide, and carbon dioxide were measured during TPD process. The TPD results showed that the decomposition reaction proceeded in several stages over the temperature range studied.

Theoretically, the $(NH_4)_6Mo_7O_{24}{\cdot}4H_2O$ in the Mo-lignin sample would first decompose gradually into MoO_3. As Biedunkiewicz et al. proposed, there were four stages for the thermal decomposition of $(NH_4)_6Mo_7O_{24}{\cdot}4H_2O$ (precursor) in argon (Biedunkiewicz et al. 2014), i.e.,

Stage I $(NH_4)_6Mo_7O_{24} \rightarrow (NH_4)_4Mo_7O_{23}H_2O + 2NH_3 + 4H_2O$.

Stage II $(NH_4)_4Mo_7O_{23}H_2O \rightarrow (NH_4)_3Mo7O_{22}.5H_2O + NH_3 + 0.5H_2O$.

Stage III $(NH_4)_3Mo_7O_{22}.5H_2O \rightarrow (NH_4)Mo_7O_{21.5} + 2NH_3 + 2H_2O$.

And stage IV and stage V $(NH_4)Mo_7O_{21.5} \rightarrow 7MoO_3 + NH_3 + 0.5H_2O$.

In these stages, NH_3 were formed and released with increase of the heating temperature from 120 to 320 °C. There was a CO_2 formation peak between 220 and 350 °C, and it was suggested that ammonium molybdate was progressively variable in the decomposition process with the existence lignin, i.e., partial ammonium molybdate was reduced to MoO_2 during decomposition process by carbon active phase (C*) in lignin through the possible reaction:

$$(NH_4)_6Mo_7O_{24} \cdot 4H_2O + C^* \rightarrow MoO_2 + NH_3 + CO_2 + H_2O$$

The most significant CO_2 formation was observed between 350 and 790 °C, and this might be due to the gradual reduction of molybdenum oxides to metallic Mo by carbon active species (C*) and/or the formed CO through the following possible reactions:

$$2MoO_3 + C^* \rightarrow 2MoO_2 + CO_2$$
$$MoO_3 + C^* \rightarrow MoO_2 + CO$$
$$MoO_3 + CO \rightarrow MoO_2 + CO_2$$
$$MoO_2 + 2C^* \rightarrow Mo + 2CO_2$$
$$MoO_2 + 2CO \rightarrow Mo + 2CO_2$$

The formation peaks of CO, H_2S and CH_4 between 350 and 500 °C were produced by the decomposition of kraft lignin through the reaction of $CxHyOz \rightarrow CO + CO_2 + CH_4$. The major CO peak from 550 to 750 °C was attributed to the carbothermal reduction of MoO_2 in the lignin char matrix.

$$MoO_2 + 2C^* \rightarrow Mo + 2CO$$

Then, the reduced molybdenum further reacts with carbon active species to form Mo2C.

$$2Mo + C^* \rightarrow Mo_2C$$

The major CO and CO_2 peaks at 950 °C were attributed to the catalytic carbonization of lignin char by

Mo_2C. Hydrogen was generated by the cracking of CH_x ($x = 1\sim3$) groups bonded in the lignin char structures and it was noticed there were two maxima of hydrogen evolution peaks, the first one was between 490 and 860 °C with a peak temperature at 750 °C, and it was assigned to the thermal decomposition of C-H bonds in lignin char; the second one was observed in the range of 860–1000 °C, centered at 950 °C, and it was attributed to the catalytic graphitization of lignin char by molybdenum carbide.

Figure 2e shows the trend of vent gas species during TPD of the iron promoted lignin sample. NO_2 was first observed to form between 160 and 250 °C. Iron nitrate was thermally decomposed to iron(III) oxide, nitric oxide, and oxygen (Melnikov et al. 2014).

$$4\ Fe(NO_3)_3{\cdot}9H_2O \rightarrow 36H_2O + 2Fe_2O_3 + 12NO_2 + 3O_2$$

Gases like CH_4, CO, and CO_2 were detected during the thermal process. The surface functionalities chemically bound to the lignin decomposed upon heating and released gaseous compounds at different temperatures. Sharp peaks corresponding to CO_2, CO, and CH_4 were observed at ~237 °C. Of these gaseous species, more than 95% were CO_2.

Both CO_2 and CO evolution were detected over a wider temperature range of 400–1000 °C, with two peaks at about 630 and 900 °C for the Fe-kraft lignin sample. The formation of the carbon monoxide at the temperature range (450–700 °C) was probably caused by the breaking of diaryl ether groups and secondary pyrolysis of volatiles. The largest release of CO occurs around 900 °C, and was attributed to the break of diaryl ether linkages during catalytic graphitization process.

Effect of different metals on decomposition of kraft lignin

Three phases were produced during the catalytic thermal treatment of metal-promoted kraft lignin samples under an argon atmosphere: gas/aerosol, liquid (tars, condensable vapors, etc.), and solid carbon (metal free). Table 1 showed the solid carbon residue yield after catalytic thermal treatment. The yields of the solid carbon residues from kraft lignin with different transitional metals were 31.3% for iron, 31.5% for nickel, 34.0% for copper, and 30.1% for molybdenum, respectively. Thermal decomposition of Cu-lignin under argon atmosphere produced 19.2% liquid products, the greatest of which was water, compared to 18.0%, 17.8%, and 17.3% of Fe-, Mo-, and Ni-lignin, respectively. Table 1 demonstrates that decomposition of Mo-lignin under argon gives gaseous phase yield of 52.6%, (the highest) compared to 51.2%, 50.7%, and 46.8% of Ni-, Fe-, and Cu-lignin, respectively.

Characterization

Solid product-specific surface area

Table 2 lists the Brunauer-Emmett-Teller (BET) surface area (S_g) of carbon-based nano-materials from kraft lignin promoted with iron nitrate (Fe-), nickel nitrate (Ni-), copper nitrate (Cu-) ,and ammonium molybdate (Mo-) after thermal treatment at 1000 °C. It was found that the physicochemical properties of the products were different depending upon the promoting metals. The BET surface area of the solid samples obtained from different metal precursors were in the range of 88–115 m^2/g with the order of Ni- > Fe- > Mo- > Cu-. The product samples prepared from iron nitrate and nickel nitrate had higher surface area than the molybdenum and copper samples. This was because nickel and iron metal had higher activity with the cracking of C-H, C-O, and other bonding in biomass resources.

XRD

Figure 3 shows the XRD patterns of the samples from kraft lignin promoted with different transitional metals. Figure 3a is XRD of the thermal-treated Cu-lignin sample. The strong intensity diffraction peaks at 43.24°, 50.38°, and 74.03° were assigned to the (111), (200), and (220) planes of face-centered cubic (fcc) Cu crystals, respectively. The sizes of the copper nanoparticles

Table 1 Effects of transitional metals on graphene nanomaterial production at the temperature of 1000 °C for 1 h

Metal-kraft lignin precursors	Solid carbon (wt%)	Liquid (wt%)	Gas (wt%)
Fe-	31.3	18	50.7
Ni-	31.5	17.3	51.2
Cu-	34.0	19.2	46.8
Mo-	30.1	17.8	52.6

Table 2 BET surface area (S_g) of carbon-based nano-materials from kraft lignin

Sample	S_g (m^2 g^{-1})
Fe-	108
Ni-	115
Cu-	88
Mo-	93

were estimated using the Scherrer equation and the average diameter of the particles was 56.2 nm (Table 3).

Figure 3b shows XRD pattern of the heat-treated Ni-lignin sample. The peaks observed at 2θ of 44.5°, 51.8°, and 76.4° were characteristic of face-centered cubic (fcc)nickel phase, corresponding to (111), (200), and (220) planes, and these peaks indicated that the Ni had a polycrystalline structure.

The XRD pattern of the Mo-lignin sample is plotted in Fig. 3c. The diffraction peaks located at 34 3° (100), 39.6° (101), 37.8° (002), 52.3° (102), 34.4° (100), 61.5° (110), 69.8° (103), and 74.5° (112) were assigned to β-Mo2C phase (PDF 35-0787). Additionally, the average crystallite size determined by (101) peak using Scherrer formula, was 21.0 nm (Table 3).

The XRD pattern of the Fe-Lignin sample (Fig. 3d) showed three peaks at 43.50°, 50.64°, and 74.36° that corresponded to the γ-iron (111), (2 0 0), and (2 2 0) planes (PDF#98-000-0258). The

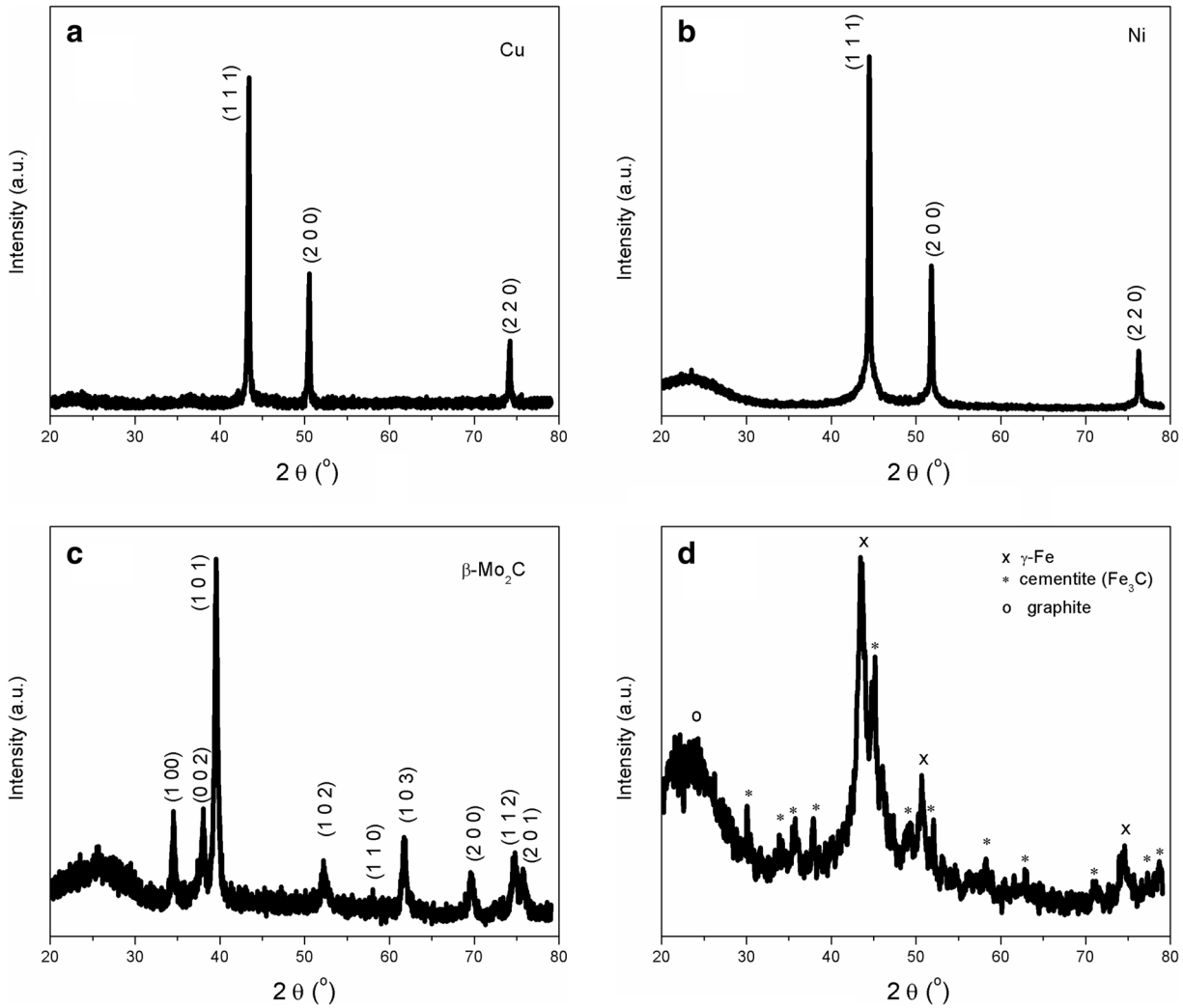

Fig. 3 XRD patterns of the samples prepared with Cu (**a**), Ni (**b**), Mo (**c**), and Fe (**d**) after heat treatment at 1000 °C under an argon flow for 1 h

Table 3 Particle size of different metals

Metal		Average particle size (nm)
Ni		52.4
Cu		56.2
Mo		21.0
Fe	γ-Fe	9.8
	α-Fe	18.5
	Fe_3C	19.7

peaks 37.75°, 40.7°, 42.6°, 43.75°, 44.56°, 44.94°, 45.86°, 49.12°, and 57.8° were assigned to cementite (Fe_3C) with correspondence planes of (1 2 1), (2 1 0), (2 0 1), (2 1 1), (1 0 2), (2 2 0), (0 3 1), (1 1 2), and (2 2 1), respectively (PDF#00-035-0772). There was a peak at 26.55° which corresponded to graphite (002) (PDF#00-056-0160) plane for all samples, meaning the graphene structure was formed from kraft lignin after thermal treated at 1000 °C.

The mean particle size, L, was calculated for the most intense diffraction peaks of each metal using the Scherrer formula (Patterson 1939). The results are shown in Table 3. Average particle sizes of these crystal phases calculated using the Scherrer formula are 52.4 nm, 56.2 nm, 21.0 nm, 18.5 nm, 9.8 nm, and 19.7 nm for Ni, Cu, β-Mo_2C, α-Fe, γ-iron, and Fe_3C, respectively.

Raman

The Raman spectra can identify the presence of graphite and disordered amorphous carbon in the samples. Figure 4 shows Raman spectra of the thermal-treated samples from kraft lignin promoted with different transitional metals. In all the as-obtained samples, two strong resonant peaks were observed, D band near 1354 cm^{-1} and G band near 1583 cm^{-1}. The band around 1354 cm^{-1} (D band) was associated with the disorder-induced scattering produced by imperfections or loss of hexagonal symmetry in the carbon structure. This band does not appear in perfect graphite crystals. Therefore, this band has been used to evaluate the degree of imperfection or crystallinity of graphite. On the contrary, the band around 1583 cm^{-1} (G band) is always observed in all graphite materials. A 2D band at ~2706 cm^{-1}, as well as a weak D + G peak at ~2920 cm^{-1}, was also observed. D to G band intensity ratio (I_D/I_G) is an important parameter for determining the defect density in graphene films. The D, G, and 2D peaks were fitted with Lorentz functions. The I_D/I_G ratio was calculated using the height of the D and G peak intensities. The crystalline size along the *a*-axis (L_a) was calculated using the Cançado equation (Pimenta et al. 2007). The I_D/I_G values of the samples prepared from kraft lignin with different transitional metals are listed in Table 4. The I_D/I_G values of the prepared samples were 1.50, 1.46, 1.39, and 1.29 for Cu-, Mo-, Ni-, and Fe- catalyzed

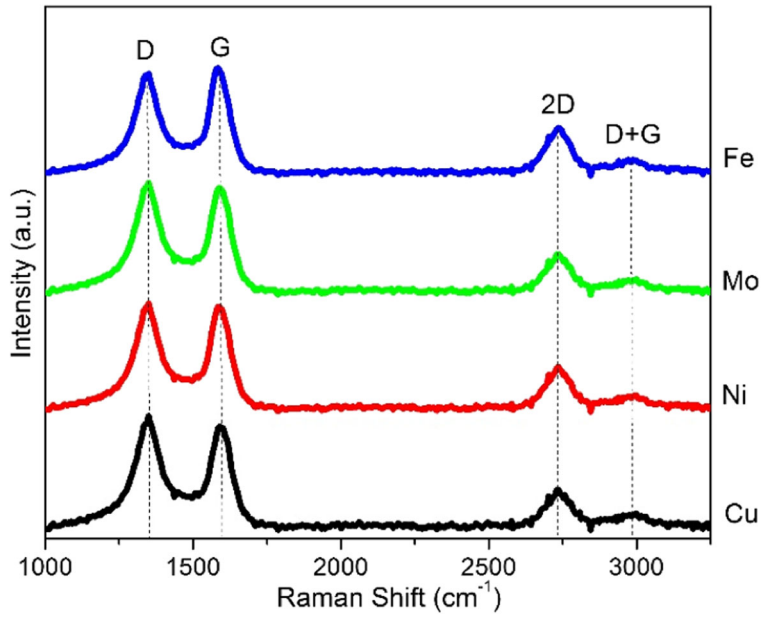

Fig. 4 Raman spectra for different metal catalysts

Table 4 Fitting results of different metal catalyst

Metal	I_D/I_G	$(I_{D+G})/2D$	L_a (nm)
Cu	1.5	0.53	12.78
Mo	1.46	0.46	13.19
Ni	1.39	0.46	13.81
Fe	1.29	0.4	14.87

kraft lignin samples, respectively. The graphitization degree of these four samples was in the order of Cu- < Mo- < Ni- < Fe-; therefore, the graphitization activity was increasing in the order of Cu < Mo < Ni < Fe. An in-plane size of the graphite crystals (L_a) in nanometers, was estimated by a ratio of the intensity of the D and G bands, I_G/I_D, using an equation, $La \approx 4.4(I_G/I_D)$. The values of L_a of the samples were given in 0. All four samples demonstrated a similar graphene crystal size of 13–15 nm.

SEM

Figure 5a, b shows SEM images of copper-promoted kraft lignin samples dried at 105 °C (a) and thermal treated at 1000 °C under an argon flow for 1 h (b). As shown in Fig. 5a, the surface of the calcined sample is smooth and clean. The surface morphologies of the thermal-treated copper kraft lignin sample (Fig. 5b) were different than the dried sample. The most obvious feature observed was formation of nanoparticles over the surface of the thermal-treated sample, where particles diameters ranged from 5 to 10 nm. More micropores and micro-channels were also observed on the surface of the thermal-treated sample.

The dried Ni-lignin sample was made of amorphous structures in different sizes (Fig. 5c, d) and Fig. 5d shows the morphology of thermal-treated nickel-lignin. The SEM image of the product in Fig. 5d shows that the shape and size of particles are quite different from the dried precursor; spherical particles were seen over the decomposed sample. The image (Fig. 5d) also shows nano-flakes uniformly distributed on the surface of the decomposed sample with sizes between 30 and 70 nm.

Figure 5e, f shows SEM images of Mo-kraft lignin samples dried at 105 °C (e) and thermal treated at 1000 °C (f). As shown in Fig. 5e, the surface of the dried sample was smooth and clean. The morphologies of the decomposed Mo-kraft lignin sample (Fig. 5f) were different than the dried sample. It was observed that the sample was composed of nanoparticles. These particles had sizes between 5 and 10 nm. XRD result (Fig. 3c) proves these nanoparticles were molybdenum carbide.

Figure 5g, h shows SEM images of Fe-kraft lignin samples dried at 105 °C (g) and thermal treated at 1000 °C (h). As shown in Fig. 5g, the surface of the dried sample is filled with porous nanoparticles. These nanoparticles had sizes ranges 2–8 nm. The decomposed Fe-kraft lignin sample (Fig. 5h) was composed of nanoparticles. Spherically shaped particles with a uniform particle size were observed for the product. These particles had sizes between 5 and 10 nm. XRD result (Fig. 3d) proved these nanoparticles were composed of α-Fe, γ-Fe, iron carbide, and graphene.

HRTEM

The morphology and structure of the decomposed samples were characterized using HRTEM and images are illustrated in Fig. 6. Figure 6a–d shows HRTEM images of the thermal-treated Cu-lignin sample which consisted of Cu@C core/shell nanoparticles (Fig. 6b). The nanoparticles had spherical shape, dark cores that were enclosed by light shells (Fig. 6b, c). Most of these carbon-encapsulated nanoparticles had core diameters about 5–10 nm and the outer shell was composed of 1–3 layers of graphene structure.

Figure 6e–h shows HRTEM images of the thermal-treated nickel-lignin sample. This sample was composed of nanoparticles and film-like porous material (Fig. 6e–h). HRTEM images showed two types of nanoparticles: the majority nanoparticles had a narrow particle size distribution in a range from 2 to 5 nm and were encapsulated with 1–3 layers of graphene. There were also some nanoparticles with quasi-spherical shape and dark cores enveloped by 5–20 layers of concentric graphene shells (Fig. 6f). The diameters of these nanoparticles ranged from 10 to 20 nm.

Figure 6i–l show HRTEM images of the thermal-treated Mo-lignin sample. It was found that Mo_2C nanoparticles with sizes ranging from 5 to 15 nm were encapsulated in 1–15 layers of graphene structure. Figure 6k shows the HRTEM image of β-Mo_2C with the d-spacing values of 0.221 nm for the (101) crystallographic planes and there were 1–3 layers of graphene over (101) plane. Figure 6l shows the HRTEM image of β-Mo_2C with the d-spacing values of 0.2595 nm for the

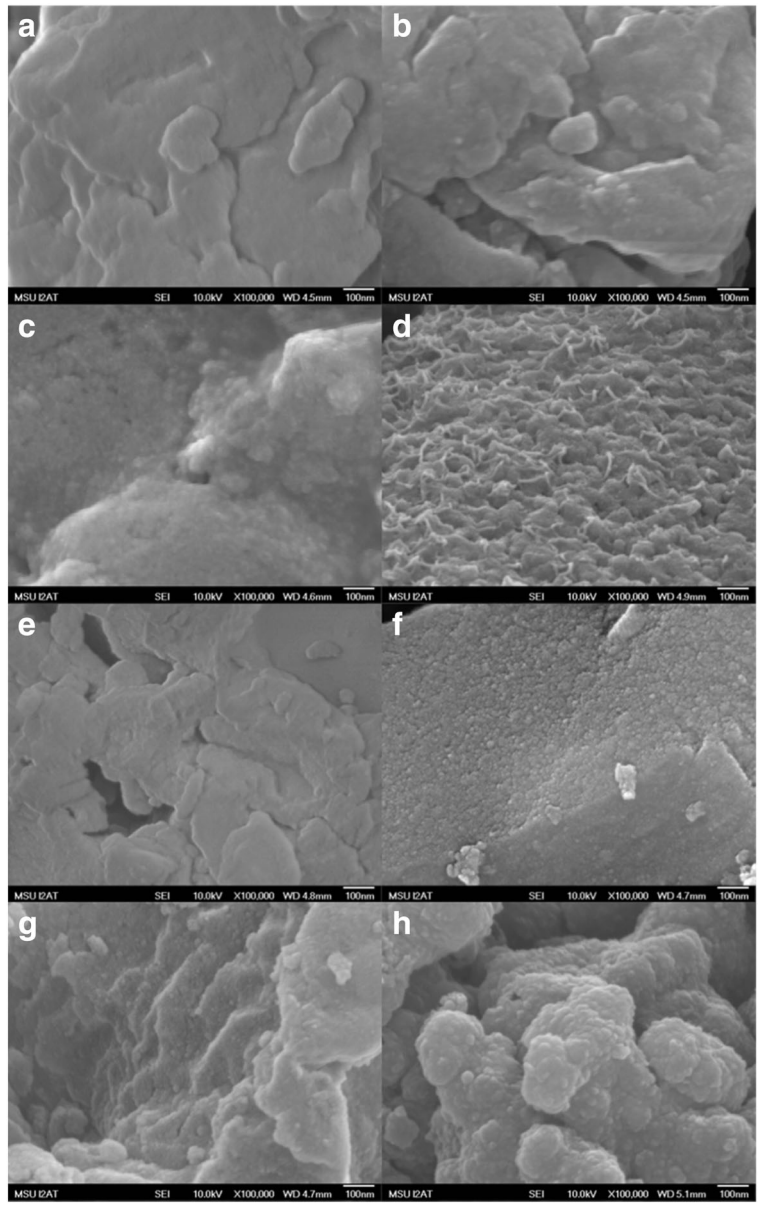

Fig. 5 SEM images of the kraft lignin samples prepared with Cu (**a**, **b**), Ni (**c**, **d**), Mo (**e**, **f**), and Fe (**g**, **h**) after heat treatment at 1000 °C under an argon flow for 1 h

(110) planes and there were more than 10 layers of graphene over (101) plane.

Figure 6m–p displays TEM images of the catalytic thermal-treated Fe-kraft lignin sample. Small and uniformly distributed iron particles were clearly seen in the sample. HRTEM images of the sample showed the nanoparticles in the sample were core-shell structure with diameter of the core nano-spheres approximately 3–5 nm. The carbon shells exhibited ordered planes of the graphene structure which were observed.

Discussion

Comparison of present and previous results

Catalytic graphitization of kraft lignin to nano-materials was investigated over four transitional metal catalysts (Ni, Cu, Fe, and Mo) through a catalytic thermal treatment process. The results obtained in the present work are summarized in Table 5. BET surface areas of samples obtained from different metal precursors were in the range of 88–115 m^2/g within the order of Ni- > Fe- >

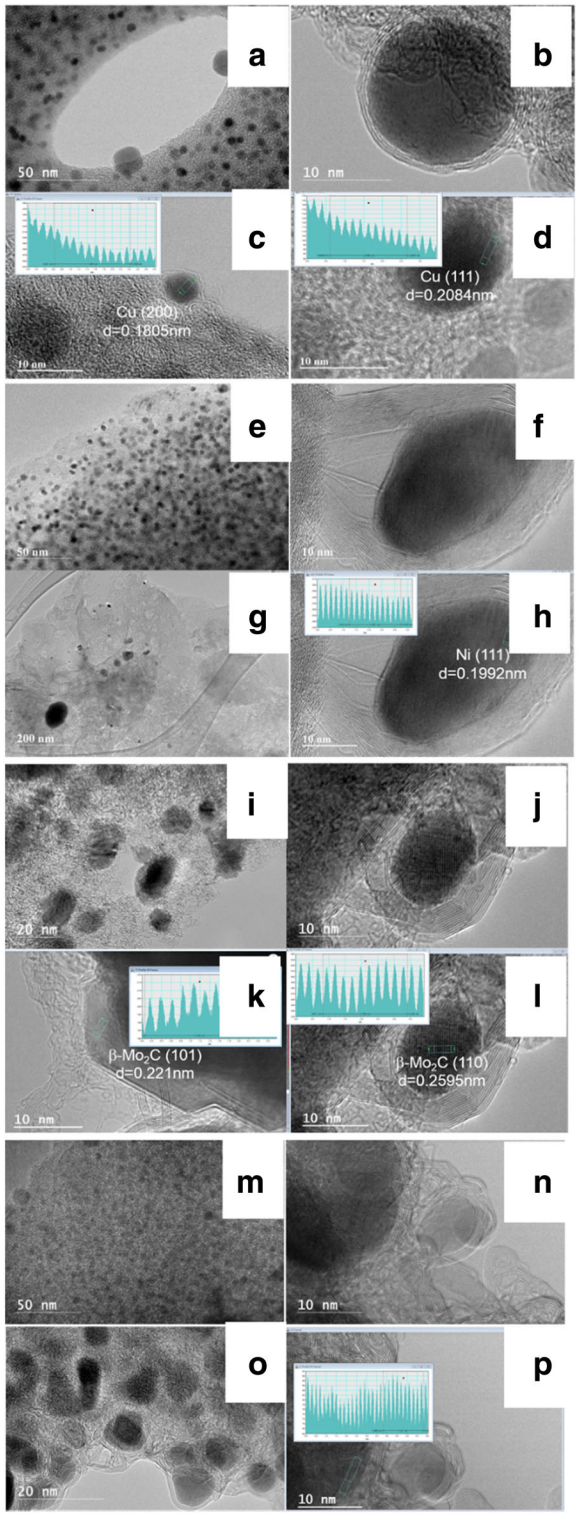

Fig. 6 HRTEM images of the kraft lignin samples prepared with Cu (**a**–**d**), Ni (**e**–**h**), Mo (**i**–**l**), and Fe (**m**–**p**) after heat treatment at 1000 °C under an argon flow for 1 h

Mo- > Cu-. Thermal gravimetric analysis (TGA) and temperature-programmed decomposition (TPD) experimental results show that adding transitional metals can promote the decomposition and carbonization of kraft lignin. The catalytic activity increased with an order of Mo≅Cu < Ni≅Fe. XRD results show that face-centered cubic (fcc) Cu crystals are formed in the thermal-treated Cu-lignin sample, fcc nickel phase for the Ni-lignin sample, β-Mo_2C hexagonal phase for the Mo-lignin sample and α-Fe, γ-iron, and cementite (Fe_3C) for the Fe-lignin sample. Average particle sizes of these crystal phases calculated using the Scherrer formula are 52.4 nm, 56.2 nm, 21.0 nm, 18.5 nm, 9.8 nm, and 19.7 nm for Ni, Cu, β-Mo_2C, α-Fe, γ-iron, and Fe_3C, respectively. Raman results prove that the graphitization activity of these four metals is in the order of Cu < Mo < Ni < Fe. Scanning electron microscopy (SEM) and high-resolution transmission electron microscopy (HRTEM) show that multi-layer graphene-encapsulated metal nanoparticles are the main products, coinciding with some graphene sheets/flakes from kraft lignin catalyzed by transitional metals. It is concluded the catalytic activity follows the order of Fe > Ni > Mo > Cu. Previously notable works on catalytic graphitization of solid carbon resources (Ōya and Ōtani 1979; Weisweiler et al. 1971; Kakunuri et al. 2016; Maldonado-Hódar et al. 2000; Demir et al. 2015; Wang et al. 2016; Yan et al. 2018; Yudasaka et al. 1997; Leng et al. 2017) are listed in Table 6.

Oya et al. (Ōya and Ōtani 1979) carried out the catalytic thermal process to graphitize 3,5-dimethylphenol-formaldehyde (3,5-DMPF) and phenol formaldehyde carbons at 2600 °C for 1 h and 3000 °C for 10 min under argon atmosphere. About 20 wt% metal (Al, Cr, Mn, Fe, Co, Ni, Ca, Ti, V, Mo, and W) was added for graphitizing 3,5-dimethylphenol-formaldehyde (3,5-DMPF) resin carbon powder. Two mechanisms were proposed for the graphite formation: the carbon dissolution-precipitation mechanism over Al, Cr, Mn, Fe, Co, and Ni, and the carbide formation-decomposition mechanism for Ca, Ti, V, Mo, and W. Catalyst (10 wt%) was mixed with the non-graphitizing phenol formaldehyde (PF) resin carbon. It was discovered that only graphitic carbon formed over Mg, Si, Ca, Cu, and Ge catalysts; while both graphitic and turbostratic carbons were observed over Al, Ti, V, Cr, Mn, Fe, Co, Ni, Mo, and W. Weisweiler et al. investigated the graphitization of monolithic glass-like carbon as catalyzed by molten metals (Weisweiler et al. 1971).

Table 5 Characterization results of the kraft lignin samples prepared with Cu, Ni, Mo, and Fe after heat treatment at 1000 °C under an argon flow for 1 h

Catalyst	Results
BET surface area (m^2/g)	Ni- (115) > Fe-(108) > Mo- (93) > Cu- (88)
XRD	Cu: face-centered cubic (fcc) Cu phase
	Ni: fcc nickel phase
	Mo: β-Mo2C hexagonal phase
	Fe: γ-iron, cementite(Fe_3C), and graphite phases
SEM	Nanoparticles formed for all the samples
TEM	Graphene-encapsulated metal particles formed for all the samples
Raman	I_D/I_G values of the prepared samples are 1.50, 1.46, 1.39, and 1.29 for Cu-, Mo-, Ni-, and Fe- catalyzed kraft lignin samples
Summary	Catalytic performance: Fe > Ni > Mo > Cu

The heat treatment temperatures (HTT) were 100 to 200 °C higher than the melting points of the metals used and the heating time was 5 min in all cases. It was reported that catalysts such as Ni, Co, Fe, Pt, Mo, Cr, and B were highly effective in catalyzing the graphitization. In the case of Mo, Cr, and B, the reaction might take place via an intermediate formation of the carbide. The mechanism of solution-precipitation was proposed utilizing Ni, Co, Fe, Pt, Mo, Cr, and B metal catalysts. Yokokawa et al. examined the catalytic graphitization of divinyl benzene polymer, furfural alcohol, or furfural using metallic catalysts including Cu, Ni, Co, Mn, Al, Ag, Zn, and Sn (Yokokawa et al. 1966). The catalytic graphitization was observed to start at temperatures between 1400 and 1500 °C. X-ray diffraction (XRD) results showed that high levels of graphite were obtained from solid carbon resources. Ishikawa and Yoshizawa studied the effects of metallic compounds on graphitization of coke at temperatures between 2000 and 2500 °C (Ishikawa and Yoshizawa 1963). Metallic catalysts were added in a metallic state, along with oxides or carbonates. Iron was the most active catalyst on the process. Kakunuri et al. reported the catalytic graphitization of resorcinol-formaldehyde (RF) xerogel at temperatures ranging from 900 to 1800 °C (Kakunuri et al. 2016). It was discovered that RF-derived carbon xerogels could be graphitized at elevated temperature of 1200 °C in the presence of metal catalyst and no graphene formed without catalyst even at temperature as high as 2500 °C. Maldonado-Hódar et al. first prepared carbon aerogels from polymerization of resorcinol with formaldehyde, then utilized catalytic graphitization of these aerogels with Cr-, Fe-, Co-, and Ni metals at temperatures between 500 and 1800 °C. The results showed that carbon aerogels were macroporous materials that maintained large pore volumes even after pyrolysis at 1800 °C. Cr and Fe were the best catalysts for graphitization of carbon aerogels (Maldonado-Hódar et al. 2000). Demir et al. produced graphitic porous carbon from lignin using a two-step process: lignin was first hydrothermal carbonized at 300 °C and 1500 psi to produce biochar; lignin-derived char was then graphitized using a metal nitrate (iron, cobalt, and manganese nitrates) catalyst at 900–1100°. It was found that cobalt and manganese were better graphitization catalysts than iron (Demir et al. 2015). Wang et al. examined the catalytic graphitization mechanism of coal-based carbon materials with light rare earth elements (Wang et al. 2016). Two different types of graphitization mechanism of light rare earth elements were proposed to catalyze the carbon materials: dissolution–precipitation and carbide formation-decomposition. It was observed light rare earth elements exerted significant influence on the microstructure and thermal conductivity of graphite.

Properties affecting the catalytic ability of metals

Several possible mechanisms have been proposed for conversion of solid carbon resources to graphite material over transition metals through high temperature treatment:

Dissolution-precipitation mechanism: the mixture of solid carbon resources and transitional metal is first thermal-treated at high temperature. The solid carbon precursors will decompose and carbonized into disorder carbons like char, while simultaneously metal precursors are reduced to metallic particles or react with carbon to form metal carbides. The metal/carbide particles

Table 6 Results and experimental conditions for the present and some previous studies on graphitization of solid carbon resources

Works	Catalysts		Raw carbon resources	Heat treatment conditions		Atmosphere	Characterization
	Metals	Loading/wt%		HTT/°C	Heating time /min		
This work	Cu, Ni, Mo, Fe	10, 20	Kraft lignin	1000	60	Ar	XRD, SEM, HRTEM, Raman
Ōya and Ōtani	B, Al, Si, Ca, Ti, V, Cr, Mn, Fe, Co, Ni, W, Ge, Mo, Mg, Cu. Zn, Cd, Sn, Sb, Pb, Bi	10	PF carbon	2600–3000	30 10		XRD, EM
	B, Ca, Al, Ti, V, Mn, Mo, Cr, Fe, Co, Mg, Si, Ge, Cu, Zn, Cd, Sn, Sb, Pb, Bi.	20	3,5-DMPF carbon				
Weisweiler et al.	Ni, Co, Fe, Pt, Cr, B, Ag, Mg, Zn, Cd, Ge, Sn, Pd, Sb, Bi, Se, Te, Pb, Si, Nb, Zr.		Glassy carbon	Temperature higher than melting point of metal by 100–200°	5	Ar	EM
Yokokawa, et al	Cu, Ni, Co, Mn, Al, Ag, Zn, Sn	5	Divinyl benzene polymer, furfural alcohol or furfural	1400–2300	30	N2	XRD
Ishikawa and Yoshizawa	Fe, V, Ti, Li, Ag, Ba, Au, Cu, Ca, Hg, Pb, Cd, K, Zn, Al, Zr, Si, Bi, Cr, W, Se, Mn, Co, Sn	0.5–3	Coke	2000–2500			XRD
Kakunuri et al.	Fe	1	Resorcinol formaldehyde	900–1800	60	Ar	Raman spectroscopy, XRD, SAXS, and HRTEM
Maldonado-Hódar et al.	Cr-, Fe-, Co-, and Ni	1	Resorcinol (R) and formaldehyde	500–1800	240	Ar	XRD, HRTEM, and Raman
Demir et al.	Mn, Co, Fe		Lignin	900–1100	180	N2	XRD, XPS, FE-SEM, FT-IR, BET
Wang et al.	Ti, Fe, La, Ce, Pr	0–10	Petroleum coke, coal-derived pitch coke, needle coke, and natural graphite	1000–2800	30–60		XRD, SEM, energy-dispersive X-ray spectroscopy, SAED, and HRTEM

are uniformly distributed in the disorder carbon matrix. Under the heating treatment temperature, the metal disorder carbons around metal particles tend to diffuse and dissolve into metal and/or metal carbide. A saturated carbon solubility of metal particles is reached after a certain period of time and under certain temperature. With temperature decrease, the metal saturated with disordered carbon will be supersaturated with carbon. Subsequently, carbon re-precipitates in the form of graphite crystals to the free enthalpy difference between the two forms of carbon, where graphite is the highly ordered carbon with the lowest Gibbs free energy while the disordered carbons have a higher activity.

Metal carbide formation-decomposition process: during the thermal treatment process, metal can react with the solid carbon precursors to form metal carbides. With increased heating treatment temperature, metal carbides can decompose to metal and graphite.

$$\mathrm{M} + \mathrm{C} \rightarrow \mathrm{MC\ (carbide)} \rightarrow \mathrm{M} + \text{Graphitizable carbon} \rightarrow \mathrm{M} + \text{graphite}$$

The dissolution-precipitation mechanism is controlled by the solubility of carbon in metal, while metal carbide formation-decomposition mechanism is affected by the formation of carbides and thermal stability of metal carbides. Considering the catalytic graphitization mechanisms, several properties are identified to govern the catalytic performance of metals, i.e., carbon solubility in metal, strength of metal-carbon bond (M-C) to form metal carbide, carbide thermal stability, and carbon content in carbides. The properties can usually be obtained from the phase diagrams. Cu-C, Ni-C, Mo-C, and Fe-C binary phases are researched in current work (ASM International 1992). Data on carbon solubility can be found from these binary phase diagrams. As far as the data gathered by us were investigated, the relation between carbon solubility and the catalytic ability of the metal was examined. The solubility of C in solid Cu is very small, and according to the newest assessment of the Cu–C equilibrium phase diagram, the maximum solubility of carbon in copper is about 0.0078 wt% at 1084.87 °C (Subramanian 1993). Nickel shows a significant carbon solubility, and in addition a high carbon diffusivity (ASM International 1992), the maximum solubility of carbon in nickel is about 0.60 wt% at 1326.5 °C. Relatively high carbon solubility makes carbon diffuse and dissolve onto the bulk of nickel particles during a standard growth; this catalyst allows one to grow graphene layers an order of magnitude faster than copper. Carbon is an interstitial impurity in Fe, and it can form a solid solution with α, γ, and δ phases of iron. As liquid iron cools past its freezing point of 1538 °C, it crystallizes into its δ allotrope, which has a body-centered cubic (bcc) crystal structure which has relatively small interstitial positions; limited carbon atoms can be dissolved in bcc δ-Fe and the maximum solubility of C is 0.09 wt% at 1493 °C. As iron cools further to 1394 °C, it changes to the γ-iron allotrope, a face-centered cubic (fcc) crystal structure (austenite); fcc structure has larger interstitial positions where significant amounts of carbon dissolved in fcc iron to form a solid solution, and the maximum solubility of C in austenite is 2.14 wt% at 1147 °C. At 912 °C and below, the iron crystal structure again becomes the bcc α-iron allotrope (ferrite), where far fewer carbon atoms can exist in the bcc structure, and the maximum solubility of C in ferrite is sharply dropped to 0.022 wt% at 727 °C.

According to the carbide formation-decomposition mechanism, transitional metal carbides play their role not only as the product but also as the intermediate during catalytic graphitization of solid carbon resources. In accordance with this mechanism, transitional metal carbides are the connection of graphite and the metal, and they are not only the products but also operate as the intermediates. During the thermal treatment process, metal can react with the solid carbon precursors to form metal carbides, and graphite is then formed through the decomposition of the metal carbides. From the phase diagrams of Cu, Ni, Mo, and Fe (ASM International 1992), only Mo and Fe can form the stable metal carbides of the four transitional metals (Cu, Ni, Mo, and Fe) studied in this work. Carbides could be both the products and the intermediates for the graphene formation process. With increasing temperature, the carbide becomes unstable and then decomposes into graphite and the metal. Three temperature zones were described for iron carbide formation (Chesnokov and Buyanov 1987): First, below 500 °C, the rate of iron carbide formation was higher than the rate of its decomposition. In the temperature between 500 and 725 °C, the rate of iron carbide formation was initially higher than that of its decomposition, but when the iron carbide phase was starting to form, the ratio of corresponding rates changed and iron carbide gradually transformed into iron and graphite. When the temperature was above 725 °C, the rate of iron carbide decomposition was higher than that of its formation; the metallic iron phase

and graphite were stable. In current work, the heating treatment temperature is 1000 °C, both iron and molybdenum carbides are formed as the products, and they may also contribute to the formation of graphene around nanoparticles under this temperature.

In summary, it is reasonable to classify the reactivity the transition metals with carbon into three groups: (i) metals having very low carbon solubility; (ii) metals which can dissolve a significant carbon; (iii) metals which may form strong chemical bonds with carbon resulting in metal carbides. As a metal of category I, copper is observed less effective to graphitize kraft lignin. This is apparently due to very low solubility of carbon failure to form a carbide, so that none of the two mechanisms described are applicable for Cu. For metals of category II (Ni and Fe), the mechanism of dissolving carbon and re-precipitating it as graphite crystals is reasonable. The solubility of carbon in these metals is relative high. Both Mo and Fe can be classified as category III elements. They can directly react with carbon to form stable carbide. However, graphite is not formed through the carbide formation-decomposition path since these carbides are highly stable under the reaction conditions. In the case of Mo, molybdenum carbide is first produced by a direct reaction of the metal with carbonaceous species in lignin during thermal treatment process, and then the carbide becomes saturated with carbon, followed by the formation of graphite re-precipitation. Similarly, iron carbide can also serve as the catalyst for graphitization of lignin through the dissolution-precipitation mechanism. From this point of view, stable metal carbides can be categorized as category II catalyst. For the carbides, the mechanism of solution and re-precipitation is applicable as well.

Activity related to d-electron

Transition metals are an important class of catalysts and their electron structures play the role in catalysis. The catalytic activity of the transition metals is a consequence of their partly filled d and f electron structure. The catalytic activity of the transition metals in any chemical process should be related to the number of vacancies in the d shell of free atoms. Transition metals can be classified into three groups by the reactivity with carbon. (i) Metals of the IB and IIB groups usually cannot react with carbon because of a completed d-electron shell. Copper atom electron configuration is [Ar] $3d^{10}$ $4s^1$, so copper has one s-orbital electron on top of a filled d-electron shell. The full d-shells in copper contribute little to interatomic interactions, which are dominated by the s-electrons through metallic bonds. Unlike metals with incomplete d-shells, copper is lacking a capability to form a covalent bond; therefore, it has relatively low catalytic activity. (ii) Both iron and nickel are in group VIII, and their electron configurations are [Ar] $3d^6$ $4s^2$ and [Ar] $3d^8$ $4s^2$, respectively. Group VIII metals have a d shell occupied by 6–10 electrons. The energy level of such configurations is hardly changed by accepting additional electrons from carbon. Therefore, these metals can react with carbon to form covalent bond and dissolve carbon. (iii) Molybdenum is in group VIB [Kr] $4d^5$ $5s^1$. Group VIB metals have five electrons in the d shell. They form strong chemical bonds with carbon resulting in the metal carbide.

TPD-MS results (Fig. 2) show significant levels of carbonaceous gases (CO, CH_4, CO_2, etc.) formed during catalytic thermal treatment process. Carbon in gas phase can also be transferred into transitional metals through gas-solid heterogeneous process by the following reactions:

$$CO + H_2 = H_2O + \quad C\ (\text{dissolved})$$
$$2CO = CO_2 + \quad C\ (\text{dissolved})$$
$$CH_4 = 2\ H_2 + \quad C\ (\text{dissolved})$$

Surface chemical absorption, dissociation, recombination, and desorption are the most important steps over active sites in heterogeneous catalysis process. The specific nature of the electron structure of the transition metals plays the dominant role in these stages. For example, the decomposition of methane consists of breaking C-H covalent bonds. This breaking may occur in the presence of electron acceptors or substances which stimulate strong electron exchange.

Copper has configuration of $3d^{10}4s^1$, its d-shells are filled, and so copper catalysts have low activity for methane dissociation. Molybdenum atoms are characterized by an outer shell $4d^5 5s^1$ configuration, which is the lowest weight of the d^n configurations. Therefore, the catalytic activity of molybdenum is low for dissociative chemisorption methane. If we consider nickel, an atom of each has the $3d^8$ $4s^2$ configuration in its free state; we may postulate that its high statistical weight of intermediate configurations is also manifested in the high value of the electronic specific heat of this metal. The presence of configurations of the type found in nickel, which has the tendency to attract or give up electrons to form stable states, is responsible for the high

catalytic activity. An even higher activity in the dissociation of methane is exhibited by iron which has a lower statistical weight of intermediate configurations than that found in nickel. The highest activity of iron supports the hypothesis of the participation of iron carbide, which is undoubtedly formed in the catalytic process.

From the d-electron configuration, the catalytic performance for the four studied transitional metals has an order of Fe > Ni > Mo≥Cu agrees with the results of current work on catalytic graphitization of kraft lignin.

Conclusions

Catalytic graphitization of kraft lignin to nano-materials was investigated utilizing Ni, Cu, Fe, and Mo. The catalytic activity increased with an order of Mo≅Cu < Ni≅Fe. Scanning electron microscopy (SEM) and high-resolution transmission electron microscopy (HRTEM) show that multi-layer graphene-encapsulated metal nanoparticles are the main products produced in conjunction with some graphene sheets/flakes from kraft lignin catalyzed by transitional metals. The particle sizes and graphene shell layers are significantly affected by the promoted metals. Metal properties like catalytic activity, carbon solubility, and tendency of metal carbide formation are related to the graphene-based structure formation during catalytic graphitization of kraft lignin process.

Acknowledgments The authors would like to acknowledge Domtar Corp., North Carolina, for providing kraft lignin for this study. The assistance of Ms. Amanda Lawrence of the Institute for Imaging & Analytical Technologies (I^2AT) at Mississippi State University is gratefully acknowledged. Thanks to Neil Gribbins of USDA, Forest Products Laboratory, for the editorial assistance.

Funding information This work was financially supported by the USDA Forest Service through Grant no. 16-JV-11111124-075.

Compliance with ethical standards

Conflict of interest The authors declare that they have no conflict of interest.

References

Aro T, Fatehi P (2017) Production and application of lignosulfonates and sulfonated lignin. ChemSusChem 10(9):1861–1877

Handbook ASM (1992) Alloy phase diagrams. ASM International 3:2–319

Bacsa RR, Cameán I, Ramos A, Garcia AB, Tishkova V, Bacsa WS, Gallagher JR, Miller JT, Navas H, Jourdain V, Girleanu M, Ersen O, Serp P (2015) Few layer graphene synthesis on transition metal ferrite catalysts. Carbon 89:350–360

Biedunkiewicz A, Krawczyk M, Gabriel-Polrolniczak U, Figiel P (2014) Synthesis of ceramics by sol–gel method in molybdenum, silicon and carbon containing systems. Thermogravimetric studies. Adv Powder Technol 25:1462–1468

Chesnokov V, Buyanov RA (1987) Mechanism for the formation of carbon deposits from benzene on iron and nickel. Kinet Catal 28:403–407

Demir M, Kahveci Z, Aksoy B, Palapati NKR, Subramanian A, Cullinan HT, El-Kaderi HM, Harris CT, Gupta RB (2015) Graphitic biocarbon from metal-catalyzed hydrothermal carbonization of lignin. Ind Eng Chem Res 54:10731–10739

Derbyshire FJ, Presland AEB, Trimm DL (1975) Graphite formation by the dissolution—precipitation of carbon in cobalt, nickel and iron. Carbon 13:111–113

Doherty WOS, Mousavioun P, Fellows CM (2011) Value-adding to cellulosic ethanol: lignin polymers. Ind Crop Prod 33(2): 259–276

Ishikawa T, Yoshizawa S (1963) Catalyst on graphitization of carbon (II) - catalytic actions of various metallic elements. J Chem Soc Japan Ind Sect 66:14–18

Kakunuri M, Kali S, Sharma CS (2016) Catalytic graphitization of resorcinol-formaldehyde xerogel and its effect on lithium ion intercalation. J Anal Appl Pyrolysis 117:317–324

Leng W, Barnes HM, Yan Q, Cai Z, Zhang J (2017) Low temperature synthesis of graphene-encapsulated copper nanoparticles from kraft lignin. Mater Lett 185(15):131–134

Maldonado-Hódar FJ, Moreno-Castilla C, Rivera-Utrilla J, Hanzawa Y, Yamada Y (2000) Catalytic graphitization of carbon aerogels by transition metals. Langmuir 16(9):4367–4373

Melnikov P, Nascimento VA, Arkhangelsky IV, Zanoni Consolo LZ, Oliveira LCS (2014) Thermal decomposition mechanism of iron(III) nitrate and characterization of intermediate products by the technique of computerized modeling. J Therm Anal Calorim 115:145–151

Mun S.P., Cai Z., Zhang J., Fe-catalyzed thermal conversion of sodium lignosulfonate to graphene, 2013

Otani S, Fukuoka Y, Igarashi B, Sasaki K (1969) Method for producing carbonized lignin fiber. U.S. Patent 3,461,082

Ōya A, Marsh H (1982) Phenomena of catalytic graphitization. J Mater Sci 17:309–322

Ōya A, Ōtani S (1979) Catalytic graphitization of carbons by various metals. Carbon 17:131–137

Patterson A (1939) The Scherrer formula for X-ray particle size determination. Phys Rev 56(10):978–982

Pimenta MA, Dresselhaus G, Dresselhaus MS, Cançado LG, Jorio A, Saito R (2007) Studying disorder in graphite-based systems by Raman spectroscopy. Phys Chem Chem Phys 9: 1276–1290. https://doi.org/10.1039/B613962K

Ruiz-Rosas R, Valero-Romero MJ, Salinas-Torres D, Rodríguez-Mirasol J, Cordero T, Morallón E, Cazorla-Amorós D (2014) Electrochemical performance of hierarchical porous carbon materials obtained from the infiltration of lignin into zeolite templates. ChemSusChem 7:1458–1467

Subramanian PR (1993) Phase diagrams of binary copper alloys (monograph series on alloy phase diagrams), ASM International. https://www.amazon.com/Diagrams-Binary-

Copper-Alloys-Monograph/dp/0871704846 (accessed January 18, 2017)

Suhas, Carrott PJM, Ribeiro Carrott MML (2007) Lignin – from natural adsorbent to activated carbon: a review. Bioresour Technol 98:2301–2312

Wang R, Lu G, Wenming Q, Yu J (2016) Catalytic graphitization of coal-based carbon materials with light rare earth elements. Langmuir 32(34):8583–8592

Wang R, Lu G, Zhuang H, Yu J (2017) Synergistic catalytic effect of light rare earth element and other additives on the degree of graphitization and properties of graphite. J Mater Sci 52: 663–673

Weisweiler W, Subramanian N, Terwiesch B (1971) Catalytic influence of metal melts on the graphitization of monolithic glasslike carbon. Carbon NY 9:755–761

Yan Q, Zhang X, Li J, Hassan EB, Wang C, Zhang J, Cai Z (2018) Catalytic conversion of Kraft lignin to bio-multilayer graphene materials under different atmospheres. J Mater Sci 53(11):8020–8029

Yokokawa C, Hosokawa, Takegami KY (1966) Low temperature catalytic graphitization of hard carbon. Carbon 4:459–465

Yudasaka M, Tasaka K, Kikuchi R, Ohki Y, Yoshimura S, Ota E (1997) Influence of chemical bond of carbon on Ni catalyzed graphitization. J Appl Phys 81:7623–7629